Results in Chemistry 4 (2022) 100667

Contents lists available at ScienceDirect

Results in Chemistry

journal homepage: www.sciencedirect.com/journal/results-in-chemistry

DFT studies of the redox behavior of oligo(aza)pyridines and experimental CVs of 4′-substituted terpyridines

Nandisiwe Ghandi Sibongile Mateyise [a,3], Marrigje Marianne Conradie [a,*,2], Jeanet Conradie [a,b,*,1]

[a] Department of Chemistry, University of the Free State, P.O. Box 339, Bloemfontein 9300, South Africa
[b] Department of Chemistry, UiT – The Arctic University of Norway, N-9037 Tromsø, Norway

ARTICLE INFO

Keywords:
Terpyridine
Bipyridine
Phenanthroline
Reduction potential
DFT

ABSTRACT

The cyclic voltammograms of a series of substituted terpyridine ligands are presented, showing that reduction occur generally below −2 V *versus* the redox potential of ferrocene. Density functional theory (DFT) calculated energies and the theoretically calculated reduction potentials of a large series of substituted oligo(aza)pyridine ligands (terpyridine, bipyridine and phenanthroline) are determined and related to experimentally measured reduction potentials. A linear relationship is observed for the reduction potential of tpy ligands and the sum of the Hammett constant of the substituents on the ligands. It was found that the reduction potential of terpyridines relate linearly with various DFT calculated energies. It was further demonstrated that different oligo(aza)pyridines, namely phenanthrolines, bipyridines and the terpyridine ligands of this study, follow the same "reduction potentials – DFT energies" relationships.

1. Introduction

Oligo(aza)pyridines (Scheme 1) are an important class of ligands that coordinate to many transition metals. These oligo(aza)pyridine ligands and their metal complexes have applications in many fields of chemistry, such as supramolecular chemistry [1,2], molecular electronics, homogeneous [2] and redox [3] catalysis [4], fluorescence [5], photochemistry [6], biomedical applications, light-emitting devices, nonlinear optical (NLO) materials [7], photosensitizers in dye-sensitized solar cells (DSSC) [8], redox and photochemistry [9,10]. The free ligands are reduced at potentials more than 2 V below the redox couple of free ferrocene [11,12]. New 2,2′:6′,2″-terpyridine ligands with different substituent groups to tailor them for specific applications, are continuously being synthesized [13–15] and theoretically designed [7,16]. The reactivity of metal complexes containing substituted oligo(aza)pyridine ligands are related to the properties of the ligands [17], including the redox activity of the ligands [11]. It is thus of importance to find descriptors (e.g. Hammett substituent parameters, Lever's additive electrochemical parameters, pK_a's, theoretically calculated energies) that correlate to the redox activity of substituted oligo(aza)pyridine ligands and therefore also to the redox activity of their metal complexes.

There are a couple of examples in literature where the redox potentials of homoleptic transition-metal complexes containing substituted 2,2′:6′,2″-terpyridine (tpy) ligands, $[M(tpy)_2]^{2+}$ complexes, correlate well to the sum of the Hammett parameters of the tpy substituents, for M = Mn [18,19], Fe [17–19], Co [17,18], Ni [18] and Zn [18]. Both the metal- and ligand-based reductions of iron(II) and cobalt (II) complexes of tris-azinyl analogues of tpy correlates well with Lever's additive electrochemical parameters for the heterocyclic donor groups [20], as well as with sum of the pK_a's of the different ligand donor groups of the tris-azinyl ligands [20]. The metal-based reductions of cobalt(II) complexes with substituted bidentate (phenanthrolines and bipyridines) and tridentate (terpyridines) oligo(aza)pyridine ligands correlates with the pK_a of uncoordinated substituted bidentate and tridentate oligo(aza)pyridine ligands [11,21]. The phenanthroline-ligand-based reduction potential of ruthenium(II) complexes containing 1,8-bis (2-pyridyl)-3,6-dithiaoctane and substituted 1,10-phenanthrolines, related to the the pK_a of free phenanthrolines with a correlation

* Corresponding authors.
E-mail addresses: conradiemm@ufs.ac.za (M.M. Conradie), conradj@ufs.ac.za (J. Conradie).
[1] ORCID: 0000-0002-8120-6830.
[2] ORCID: 0000-0001-8104-7684.
[3] ORCID: 0000-0002-8671-5765.

https://doi.org/10.1016/j.rechem.2022.100667
Received 30 September 2022; Accepted 15 November 2022
Available online 17 November 2022

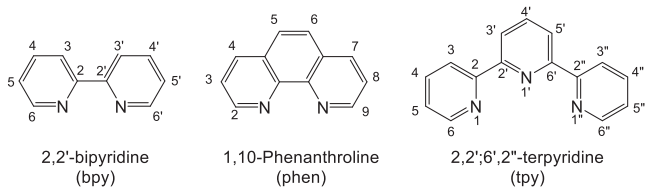

Scheme 1. Structure and atom numbering scheme of the oligo(aza)pyridine ligands of this study. The tpy ligands are shown in Scheme 2 and the bpy and phen ligands are tabulated in Table 2.

coefficient $R^2 = 0.94$ [22].

Density functional theory (DFT) calculated energies (e.g. lowest unoccupied molecular orbital (LUMO) energy, electron affinity, global electrophilicity index, Mulliken electronegativity) of substituted phenanthrolines revealed a strong correlation to reduction potential of the same ligands [11]. DFT calculated energies of metal complexes containing substituted oligo(aza)pyridines (phenanthrolines and bipyridines) revealed a strong correlation to metal-based oxidation potential of the same molecules for metal = Fe [23,24], Ru [25], Os [26], Mn [27], Co [28] and Cu [29]. It was demonstrated that the DFT calculated LUMO energies of a simplified model system of aryl substituted 4′-aryl-tpy ligands, namely aryl-pyridine molecules, revealed a strong correlation to the Hammett parameters of the substituents. In addition, the sum of the Hammett parameters of the substituents on 4′-aryl-tpy correlated to the electrochemical data of metal complexes containing substituted 4′-aryl-tpy, $[M(4'\text{-aryl-tpy})_2]^{2+}$ complexes, for M = Mn, Fe, Co, Fe and Zn [18], suggesting DFT calculated energies of simplified systems may be used to predict the redox potentials of larger metal-containing molecules.

Redox potentials of many metal complexes containing substituted oligo(aza)pyridines are published (e.g. Fe [6,17–19,23,24], Ru [5,25], Os [5,26], Mn [18,19,27], Co [11,17,18,21,28], Zn [18], Ni [18] and Cu [30]), but not much data in non-aqueous solvents could be found on the reduction potential of the uncoordinated oligo(aza)pyridine [11,12], that reduce at potentials c.a. 1 V lower than the reduction of coordinated oligo(aza)pyridines in metal-oligo(aza)pyridine complexes.

This contribution thus presents the experimental reduction of a series of substituted tpy ligands, see Scheme 2, as measured by cyclic voltammetry. The reduction potential of the tpy ligands, as well as data of substituted bipyridine (bpy) and phenanthroline (phen) ligands from literature [11,12], listed in Table 2, are shown to be related to theoretically calculated reactivity descriptors, using DFT calculations. The ultimate goal is to identify theoretical methods that can be used to predict the redox potentials of other substituted oligo(aza)pyridine ligands and their metal complexes.

2. Experimental

2.1. General

Liquid-state ^{1}H NMR spectra were recorded at 25.0 °C on a 300 MHz Bruker Avance DPX spectrometer using deuterated chloroform as solvent. The chemical shifts (δ) are reported in parts per million (ppm) and the spectra were referenced relative to Me_4Si internal standard at 0 ppm. Reagents were obtained from Sigma-Aldrich. Solid reagents employed in preparations were used directly without further purification. Solvents were distilled prior to use.

2.2. Synthesis of ligands

Seven 4′-substituted terpyridine ligands and the tpy analogue 2,6-di(pyrazinyl)pyridine (4,4″-N-tpy), were used to perform electrochemistry on. Three ligands were synthesised using the methods below, while the following ligands were obtained from Sigma-Aldrich: 2,2′:6′,2″-terpyridine (tpy); 4′-chloro-2,2′:6′.2″-terpyridine (4′-Cl-tpy); 4′-(4-Methylphenyl)-2,2′:6′,2″-terpyridine (4′-MePh-tpy); 4,4′,4″-Tri-*tert*-Butyl-2,2′:6′,2″-terpyridine (4,4′,4″-tBu-tpy) and 4′-(4-Chlorophenyl)-

Table 1
Electrochemical data for the substituted tpy ligands and 2,6-di(pyrazinyl)pyridine, obtained in DMF with 0.1 M TBAHFP as supporting electrolyte, at 0.100 V s^{-1}, reported in V *versus* Fc/Fc^+.

Ligand	E_{pc}	E_{onset}	Σ Hammett[a]
4′-4ClPh-tpy	−2.324	−2.230	0.12
4′-Cl-tpy	−2.299	−2.170	0.23
4,4′-N-tpy	−2.293	−2.150	–
4′-OMe-tpy	−2.677	−2.415	−0.27
4′-4MePh-tpy	−2.564	−2.390	−0.03
4′-pyrr-tpy	−2.763	−2.563	−0.83
tpy[b]	−2.630	−2.420	0.00
4,4′,4″-tBu-tpy	−2.617	−2.453	−0.60

a *para* Hammett constant, except for 4,4′,4″-tBu-tpy for which 3 × the *para* Hammett constant for ^{t}Bu was used.
b tpy in CH_3CH: E_{pc} (V vs Fc/Fc^+) = -2.584, E_{onset} (V vs Fc/Fc^+)) = -2.455.

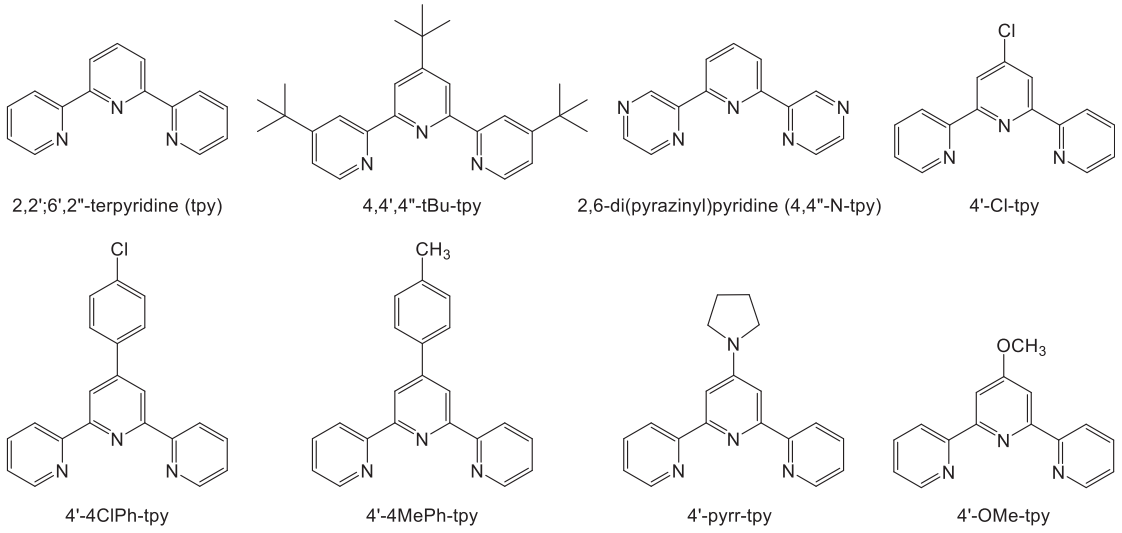

Scheme 2. Structure and abbreviations used for the substituted terpyridine ligands of this study.

Table 2
DFT data (this study) and electrochemical data at a scan rate of 0.100 V s^{-1} of the tpy ligands (this study), as well as electrochemical data of bpy and phen ligands from literature [11,12]. All data in eV except for E_{pc} and $E_{1/2}$ that is in V vs Fc/Fc^{+}. Numbering of ligand's substituents according to Scheme 1.

Ligand	$E_{pc,\ experimental}$	$E_{1/2,\ calculated}$	E_{HOMO}	E_{LUMO}	η	μ	μ^{-}	μ^{+}	ω	ω^{-}	ω^{+}
4′-4ClPh-tpy	−2.324	−2.628	−6.779	−1.819	4.960	−4.299	−5.54	−3.06	1.863	3.09	0.94
4′-Cl-tpy	−2.299	−2.680	−6.911	−1.739	5.172	−4.325	−5.62	−3.03	1.808	3.05	0.89
4,4′-N-tpy	−2.293	−2.459	−7.013	−2.047	4.967	−4.530	−5.77	−3.29	2.066	3.35	1.09
4′-OMe-tpy	−2.677	−2.852	−6.658	−1.454	5.204	−4.056	−5.36	−2.75	1.580	2.76	0.73
4′-4MePh-tpy	−2.564	−2.755	−6.623	−1.599	5.024	−4.111	−5.37	−2.85	1.682	2.87	0.81
4′-pyrr-tpy	−2.763	−3.040	−5.818	−1.201	4.617	−3.510	−4.66	−2.36	1.334	2.36	0.60
tpy	−2.630	−2.869	−6.690	−1.511	5.180	−4.100	−5.40	−2.81	1.623	2.81	0.76
4,4′,4″-tBu-tpy	−2.617	−3.027	−6.480	−1.237	5.243	−3.858	−5.17	−2.55	1.420	2.55	0.62
3,4,7,8-Me-phen	−2.635	−2.883	−6.249	−1.668	4.580	−3.958	−5.10	−2.81	1.710	2.84	0.86
2,9-Me-phen	−2.603	−2.902	−6.293	−1.604	4.689	−3.949	−5.12	−2.78	1.663	2.80	0.82
5-NH2-phen	−2.600	−2.820	−5.843	−1.696	4.147	−3.770	−4.81	−2.73	1.713	2.79	0.90
4-Me-phen	−2.577	−2.830	−6.473	−1.774	4.699	−4.124	−5.30	−2.95	1.810	2.99	0.93
5-Me-phen	−2.562	−2.879	−6.429	−1.742	4.687	−4.085	−5.26	−2.91	1.781	2.95	0.91
5,6-Me-phen	−2.550	−2.840	−6.322	−1.654	4.668	−3.988	−5.16	−2.82	1.703	2.85	0.85
phen	−2.533	−2.835	−6.574	−1.786	4.788	−4.180	−5.38	−2.98	1.824	3.02	0.93
4,7-Ph-phen	−2.393	−2.715	−6.323	−1.817	4.507	−4.070	−5.20	−2.94	1.838	3.00	0.96
5-Cl-phen	−2.321	−2.620	−6.648	−2.042	4.606	−4.345	−5.50	−3.19	2.050	3.28	1.11
5,6-O-H2-phen	−2.252	−2.587	−6.850	−1.955	4.896	−4.403	−5.63	−3.18	1.980	3.23	1.03
4,7-Cl-phen	−2.221	−2.486	−6.818	−2.223	4.595	−4.521	−5.67	−3.37	2.224	3.50	1.24
5-NO2-phen	−1.348	−1.408	−7.203	−3.070	4.133	−5.137	−6.17	−4.10	3.192	4.61	2.04
5,6-O2-phen	−0.925	−0.920	−7.265	−3.680	3.585	−5.473	−6.37	−4.58	4.177	5.66	2.92
4,4′-tBu-bpy	−2.666	−3.006	−6.699	−1.244	5.456	−3.972	−5.34	−2.61	1.445	2.61	0.62
4,4′-Me-bpy	−2.679	−2.869	−6.748	−1.412	5.336	−4.080	−5.41	−2.75	1.560	2.75	0.71
4,4′-OMe-bpy	−2.612	−2.962	−6.780	−1.218	5.562	−3.999	−5.39	−2.61	1.438	2.61	0.61
bpy	−2.542	−2.802	−6.890	−1.553	5.338	−4.221	−5.56	−2.89	1.669	2.89	0.78

2,2′:6′,2″-terpyridine (4′-ClPh-tpy). The synthesis of the following three ligands was done as described below.

2.2.1. 4′-methoxy-2,2′:6′,2′′-terpyridine (4′-OMe-tpy)

A published method was used with slight changes [17]. Small pieces of sodium (0.100 g) were added to methanol (15 ml) at room temperature. Once all the sodium reacted, solvent was removed in vacuo. Sodium methoxide was suspended in dry DMF (10 ml) and 4′-chloro-2,2′:6′,2″-terpyridine (0.248 g, 0.9264 mmol) was added. The suspension was heated at 125℃ for 4 h. After cooling to room temperature, the suspension was added into water (50 ml) and the off-white precipitate was collected by suction filtration. Spectroscopically pure 4′-methoxy-2,2′:6′,2″-terpyridine (white flakes) was obtained (0.2114 g, 75.47 %). δ_H (300 MHz, $CDCl_3$): 8.706–8.684 (2H, m, CH), 8.623 (2H, d, CH), 8.028 (2H, s, CH), 7.875–7.824 (2H, m, CH), 7.356–7.311 (2H, m, CH), 7.261 (3H, s, CH).

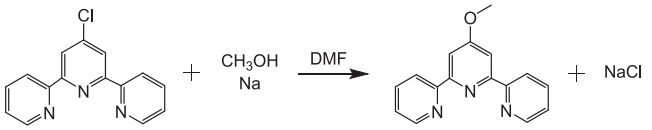

2.2.2. 4′-(N-pyrrolidinyl)-2,2′:6′,2″-terpyridine (4′-pyrr-tpy)

A published method was used with slight modifications [17]. 4′-Chloro-2,2′:6′,2″-terpyridine (0.252 g, 0.9413 mmol) was added to pyrrolidine (25 ml). The mixture was refluxed at 60–80 °C under Argon gas for 72 hrs. After cooling the solution was added to H_2O (125 ml) resulting in precipitation of the desired product. Off white solid was isolated by suction filtration and washed with distilled water (6 ml). Spectroscopically pure 4′-(N-pyrrolidinyl)-2,2′:6′,2″-terpyridine (brown powder) was obtained (0.288 g, %). δ_H(300 MHz, $CDCl_3$): 8.686–8.667 (2H, m, CH), 8.625 (2H, d, CH), 7.853–7.796 (2H, m, CH), 7.621 (2H, s, CH), 7.314–7.269 (2H, m, CH), 3.579–3.535 (4H, m, CH), 2.085–2.040 (4H, m, CH).

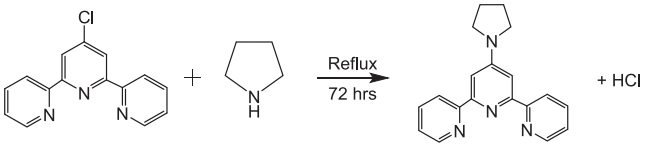

2.2.3. 2,6-di(pyrazinyl)pyridine (4,4″-N-tpy)

A published method was used with slight changes [20]. A schlenk tube was filled with 2,6-dibromopyridine (0.088 g, 0.3715 mmol), 2-(tributylstannyl)pyrazine (0.25 ml), $[Pd(PPh_3)_4]$ (0.0350 g) and dry toluene (6.5 ml) under Ar gas and heated at 110℃ to reflux for 16 hrs. Water (6.25 ml) was then added to cool the mixture. The organic layer was extracted with DCM (10 ml × 3), dried with $MgSO_4$, filtered and evaporated to dryness. The solid was suspended in *n*-pentane (10 ml), was filtered to obtain the product as yellow solid. Spectroscopically pure 2,6-di(pyrazinyl)pyridine was obtained (0.054 g, 61.78 %). δ_H (300 MHz, $CDCl_3$): 9.854 (2H, d, CH), 8.670 (4H, s, CH), 8.493 (2H, d, CH), 8.050 (1H, t, CH).

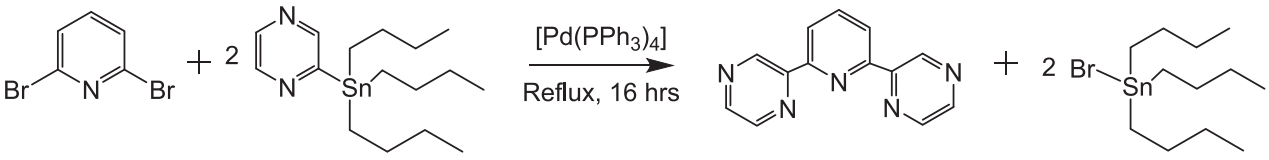

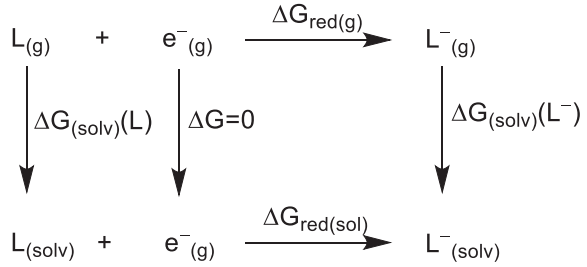

Scheme 3. Thermodynamic cycle for the absolute reduction potential of the oligo(aza)pyridine ligands L of this study. $\Delta G_{red(g)}$ and $\Delta G_{red(sol)}$ are the free energy change associated with reduction in the gas and solvent phase respectively; $\Delta G_{(solv)}(L)$ = solvation energy of L.

2.3. Electrochemistry

Cyclic voltammetric (CV) measurements were as described in a previous publication [31], namely using a BAS100B Electrochemical Analyzer linked to a personal computer, utilizing the BAS100W Version 2.3 software. A three-electrode cell was used, with a glassy carbon (surface area 0.0707 cm^2) working electrode, Pt auxiliary electrode and an Ag/AgCl (3 M NaCl sat) reference electrode (BASI P/N MF-2052). The solvent used was anhydrous DMF and the supporting electrolyte was tetra-*n*-butylammonium hexafluorophosphate (TBAHFP) (0.1 mol dm^{-3}). A purified Ar gas blanket was employed and all measurements were taken at 25 °C. The concentration of the different samples was ca 0.002 mol dm^{-3}. Scan rates were varied between 0.05 V s^{-1} and 1.00 V s^{-1}. Repetitions with the same experimental conditions showed all reduction potentials were reproducible within 0.01 V. The working electrode was polished on a Bühler polishing mat, first with 1 μm and then with ¼ micron diamond paste (in a figure-of-eight motion), rinsed with acetone and dried before each experiment. Ferrocene was used as an internal standard and cited potentials were referenced against the Fc/Fc^+ couple, as suggested by IUPAC [32]. E_{pc} = peak cathodic potential and i_{pc} = peak cathodic current.

2.4. DFT methods

Density functional theory (DFT) calculations were performed using the Gaussian 16 program [33]. The B3LYP functional (with the Becke 88 exchange functional [34] in combination with the LYP correlation functional [35]) and the triple-ζ basis set 6–311 + G(2df,2p) was used. Optimizations were performed in gas phase. The input coordinates for the compounds were constructed using Chemcraft [36]. From the optimized gas phase output files, the energies of the highest occupied molecular orbital (HOMO), E_{HOMO}, and the lowest unoccupied molecular orbital (LUMO), E_{LUMO}, were obtained. These frontier molecular orbital (FMO) energies give, according to Koopmans theorem, an approximation of the ionization potential (IP) [37] and electron affinity (EA) [38]:

$IP = -E_{HOMO}$

$EA = -E_{LUMO}$

Using the FMO energies as approximation of the EA and IP, the following calculated reactivity and response indexes and descriptors

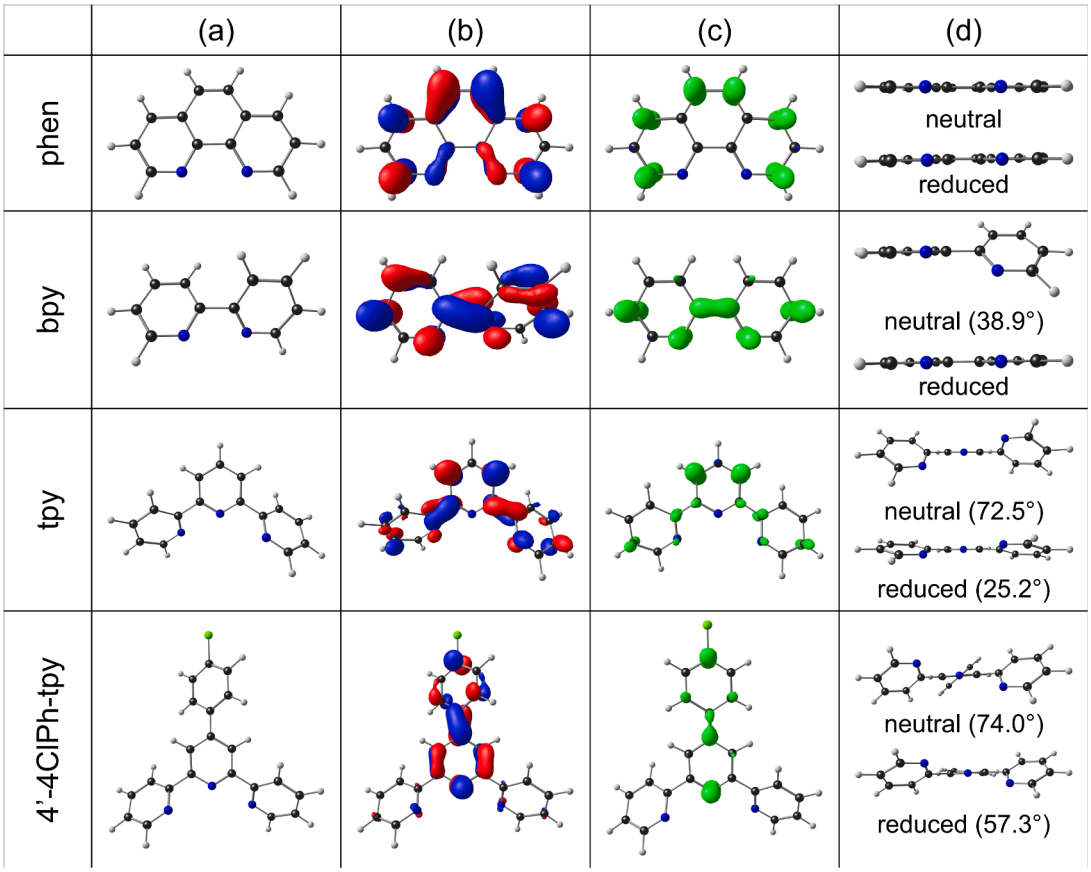

Fig. 1. B3LYP gas phase calculated (a) geometry and (b) LUMO of the indicated neutral ligands and (c) spin density plot of the indicated reduced ligands, showing the locus of the unpaired electron added upon reduction. (d) Comparison of the twisting of the pyridine rings in the neutral (top) and reduced (bottom) ligand. The dihedral angle between the non-*co*-planar pyridine rings are indicated. Contours of 0.05 e/Å^3 and 0.008 e/Å^3 were used for the MO and spin plots respectively. Colour code of the atoms (online version): N (blue), C (grey), Cl (green), H (white). (For interpretation of the references to colour in this figure legend, the reader is referred to the web version of this article.)

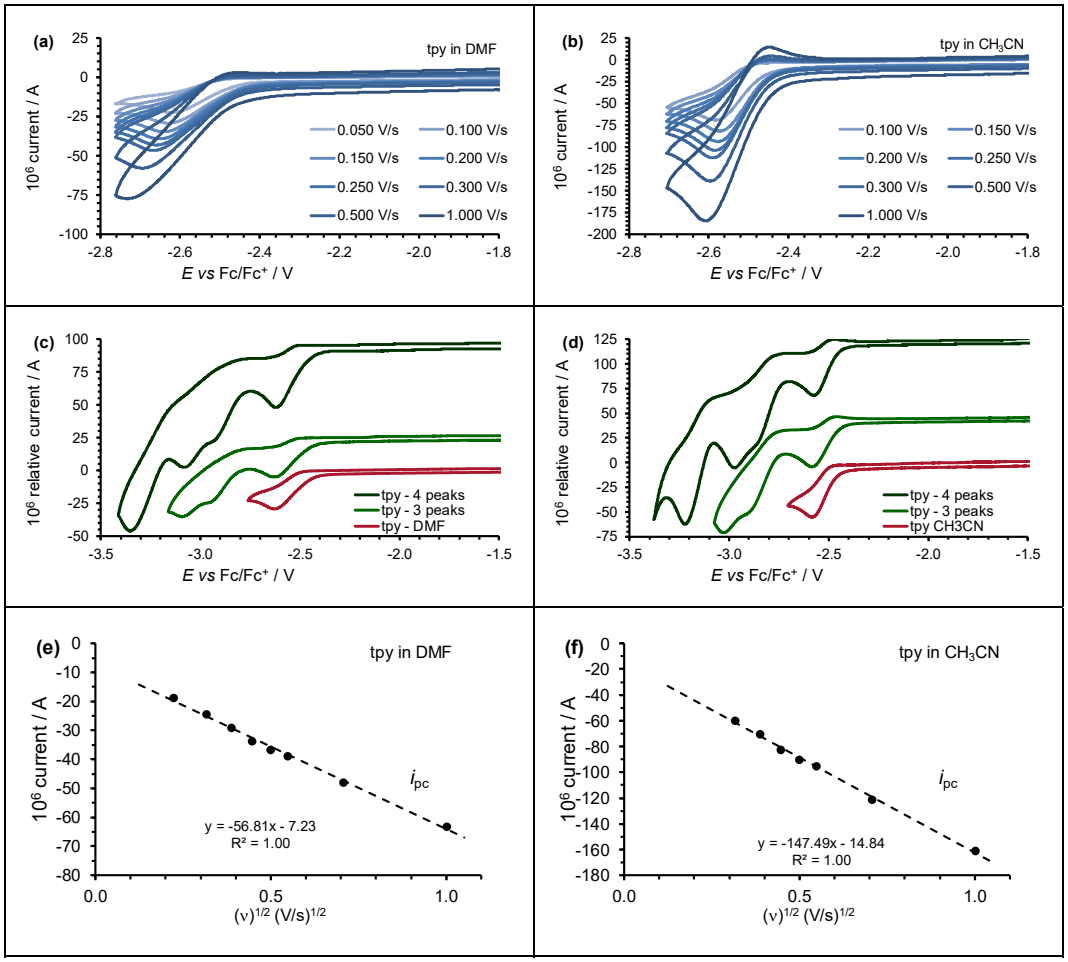

Fig. 2. CVs of tpy with 0.1 M TBAHFP as supporting electrolyte, at the indicated scan rates, reported *versus* Fc/Fc^+ in (a) DMF (0.002 M) and (b) CH_3CN (0.004 M) as solvent. CVs over different potential ranges of tpy in (c) DMF and (d) CH_3CN as solvent at a scan rate of 0.100 V s^{-1}. Relationship between peak reduction current and the square root of the scan rate (Randles–Ševčík equation) for tpy in (d) DMF and (e) CH_3CN as solvent.

were calculated using the following formulae [39–44]:

Mulliken electronegativity: $\chi = (IP + EA)/2$

chemical potential: $\mu = -(IP + EA)/2 = -\chi$

chemical hardness: $\eta = IP - EA$

global electrophilicity index: $\omega = (\mu^2/2\eta)$

chemical potential governing charge donating process: $\mu^- = -(1/4)(3IP + EA)$

chemical potential governing charge accepting process: $\mu^+ = -(1/4)(IP + 3EA)$

electro-donating power: $\omega^- = (\mu^-)^2/2\eta$

electro-accepting power: $\omega^+ = (\mu^+)^2/2\eta$

as also described in our previous publications [45,46].

To theoretically calculate the adiabatic electron affinity (EA) of ligand L, the gas phase energy difference between the neutral (E(L)) and reduced ligand ($E(L^-)$) are used:

$EA(L) = E(L^-) - E(L)$

To theoretically calculate the absolute redox potential, $E_{red,calculated,absolute}$, for the reduction of the oligo(aza)pyridine ligands of this study, the following thermodynamic equation was used:

$$E_{red,calculated,absolute} = \frac{-\Delta G_{red(sol)}}{nF}$$

Here n is the number of transferred electrons during the reduction reaction, F is the Faraday constant and $\Delta G_{red(sol)}$ the free energy of the reduction reaction in the experimental solvent. $\Delta G_{red(sol)}$ was obtained from using a thermodynamic cycle similar as what was reported in literature to determine the absolute reduction potential of the standard hydrogen electrode [47]. Scheme 3 show the thermodynamic cycle used to determine $\Delta G_{red(sol)}$ for the oligo(aza)pyridine ligands of this study. The absolute redox potential was converted to a relative redox potential *versus* the Ferrocene/Ferrocenium (Fc/Fc^+) couple, by subtracting the calculated absolute reduction potential of Fc/Fc^+ from the calculated absolute redox potential:

$$E_{\text{red,calculated vs } Fc/Fc^+} = \frac{-\Delta G_{red(sol)}}{nF} - E_{Fc/Fc^+}$$

Reported high level ab initio calculated absolute reduction potential of Fc/Fc^+ is 4.988, 4.927, and 5.043 V in acetonitrile, 1,2-dichloroethane, and dimethylsulfoxide solutions, respectively [48].

Redox calculations were done on the same level of theory as the geometry optimizations, using energies and free energies obtained by gas phase B3LYP/6–311 + G(2df,2p) optimization and frequency calculations. Single point calculations in solvent (CH_3CN or DMF) were performed using the Polarizable Continuum Model (PCM) [49] solvent model, IEFPCM [50], in Gaussian, on the same level of theory.

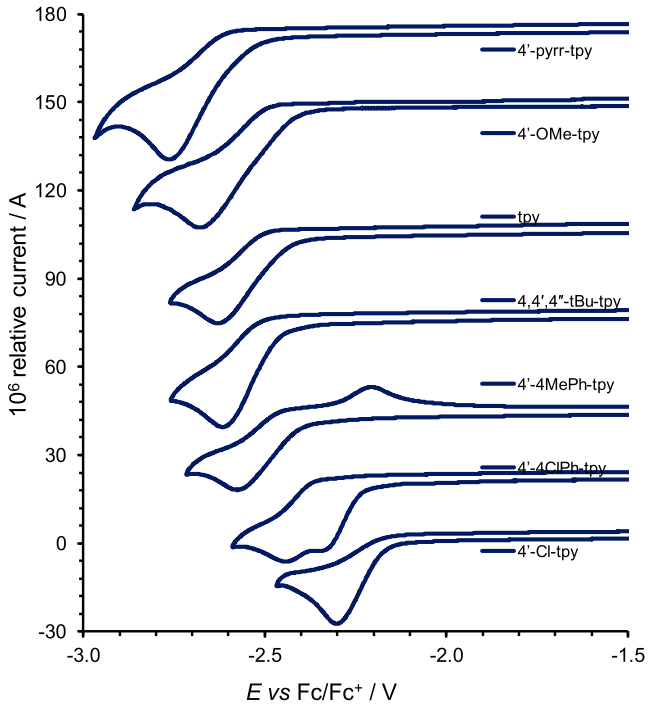

Fig. 3. CVs at a scan rate of 0.100 V s^{-1} of ca 0.002 M DMF solution containing the indicated 4′-substituted tpy ligands with 0.1 M TBAHFP as supporting electrolyte, reported *versus* Fc/Fc^{+}. Scans were done at room temperature, 25 °C.

3. Results and discussion

3.1. DFT results

The optimized geometries of the unsubstituted phen, bpy and tpy, as well as 4′-4ClPh-tpy are shown in Fig. 1. The neutral phen ligand is flat, while the pyridine rings are twisted relative to each other in bpy and tpy. For 4′-4RPh-tpy (R = Me or Cl) ligands, it is found that the central pyridine ring, the phenyl ring and the other two pyridines are twisted relative to each other, Fig. 1 (d). Upon reduction the bpy, tpy and 4′-4RPh-tpy ligands become more flat, see Fig. 1 (d). Reduced bpy is totally flat, the dihedral between the side pyridines in tpy decrease from 72.5° (neutral) to 25.2° in the reduced tpy. For reduced 4′-4RPh-tpy the central pyridine ring and the phenyl ring become co-planar, while the other two pyridines are still twisted relative to each other (57.3°), though less tilted than in the neutral ligand (74.0°). The more flat reduced ligands enhance the electron communication through the reduced ligands. The LUMO of the neutral ligand is the MO where the electron is added upon reduction. The character of the LUMO, Fig. 1 (b) thus shows the locus of the added electron, that is of the same character as the HOMO (not shown) of the reduced ligand, the locus of the added electron if no MO rearrangement upon reduction occur [51]. The spin density Fig. 1 (c) of the reduced ligand visualize the locus of the added electron upon reduction. The neutral ligand's LUMO, the reduced ligand's HOMO and the reduced ligand's spin density plots are all of similar π character.

Upon evaluation of the distribution of the added unpaired electron over the reduced ligand, see spin density plots in Fig. 1 (c), different tendencies are observed. For reduced bpy there is 0.13 e^{-} on each nitrogen- and for reduced 4′-4ClPh-tpy there is 0.24 e^{-} on the central nitrogen, while reduced phen and reduced tpy has less than 0.001 and 0.04 e^{-} on the nitrogens respectively. For reduced phen, reduced bpy and reduced tpy, the spin density is distributed over all the pyridine rings, while for 4′-4ClPh-tpy the spin density if distributed over the central flat part of the reduced ligand, namely the central pyridine and phenyl ring. The different spin density profiles of the reduced ligands suggest that the position and type of substituent groups on the different ligands, as well as the type of ligand, determine electronic and resonance effects of the substituent groups on the ligands, thereby influencing the ease of reduction of the ligand.

3.2. CV results

The electrochemical activity of the substituted phen ligands and the substituted bpy ligands, using cyclic voltammetry, was reported previously [11,12]. Here we present the observed electrochemical behaviour of tpy and substituted tpy ligands. The CVs of unsubstituted tpy, obtained at different scan rates in DMF and acetonitrile as solvents, are shown in Fig. 2. An irreversible reduction process is observed at a potential below −2.4 V *versus* Fc/Fc^{+}. The reduction peak is broad. The first irreversible reduction is followed by more irreversible reduction events, see Fig. 2 (c) and (d). The first reduction peak is broader in DMF than in CH_3CN as solvent; the difference between the onset potential (the potential in an electrochemical cell that drives the electrochemical reaction) and the peak reduction potential is 0.21 and 0.13 V for DMF and CH_3CN respectively (0.100 Vs^{-1} scan, see data in Table 1). The amount and rate of change in the geometry during reduction form the neutral form to a more flat reduced form (Fig. 1 (d)), could contribute to the slow reduction process as observed by the broad reduction peaks.

Upon reduction an unstable reduced radical anion is formed with unpaired electron distribution as shown in Fig. 1 (c). Most of the unstable radical anions formed in the electrochemical cell, decompose and diffuse away from the working electrode, before re-oxidation can take place. No re-oxidation peak is observed for the first reduction of tpy in DMF, while in CH_3CN a small re-oxidation peak appears at higher scan rates, though with large peak current voltage separations $\Delta E > 0.13$ V. However, when tpy is coordinated to a metal, a reversible tpy ligand-based reduction (of the coordinated tpy ligand), is reported for various bis-terpyridine-metal(II) complexes [12,23,27]. The peak reduction current of the first reduction is directly proportional to the square root of the scan rate as described by the Randles–Ševčík equation, indicating a diffusion controlled reduction [52] for tpy, see Fig. 2 (e) and (f).

All the substituted tpy ligands did not dissolve in CH_3CN, therefore the CVs of the substituted tpy ligands are presented in DMF here. In Fig. 3 CVs of the substituted tpy ligands at a scan rate of 0.100 V s^{-1}, obtained in DMF as solvent, are compared, while in Fig. 4 CVs obtained at different scan rates in DMF for the substituted tpy ligands and 2,6-di(pyrazinyl)pyridine are presented, with selected data in Table 1. Ligands with electron withdrawing substituents such as 4′-Cl and 4′-4ClPh, have reduction potentials more than 0.3 V more positive than that of unsubstituted tpy. Ligands with electron donating substituents such as 4′-OMe and 4′-pyy, have reduction potentials more negative than that of unsubstituted tpy. All ligands have broad irreversible reduction peaks, with more irreversible reduction events at lower potentials (not shown), as observed for tpy. For 4′-4ClPh and 2,6-di(pyrazinyl)pyridine, the first and second reduction peaks are closely overlapping.

3.3. Relationships involving reduction potentials of tpy ligands

The electronic effect of different substituents on the tpy ligands can be describe by the combined Hammett constant values of the substituents [53]. A general linear trend is obtained for the reduction potential – Hammett constant relationship, see Fig. 5 (a). The relationship between the onset potential of the reduction process with the combined Hammett constant values of the substituents, gave a higher correlation coefficient $R^2 = 0.75$, than the peak current reduction potential – Hammett constant relationship with $R^2 = 0.64$. However, a even better correlation is obtained between the DFT calculated LUMO energy and the combined Hammett constant values of the substituents, $R^2 = 0.86$, see Fig. 5 (b). The poorer relationship of the combined Hammett

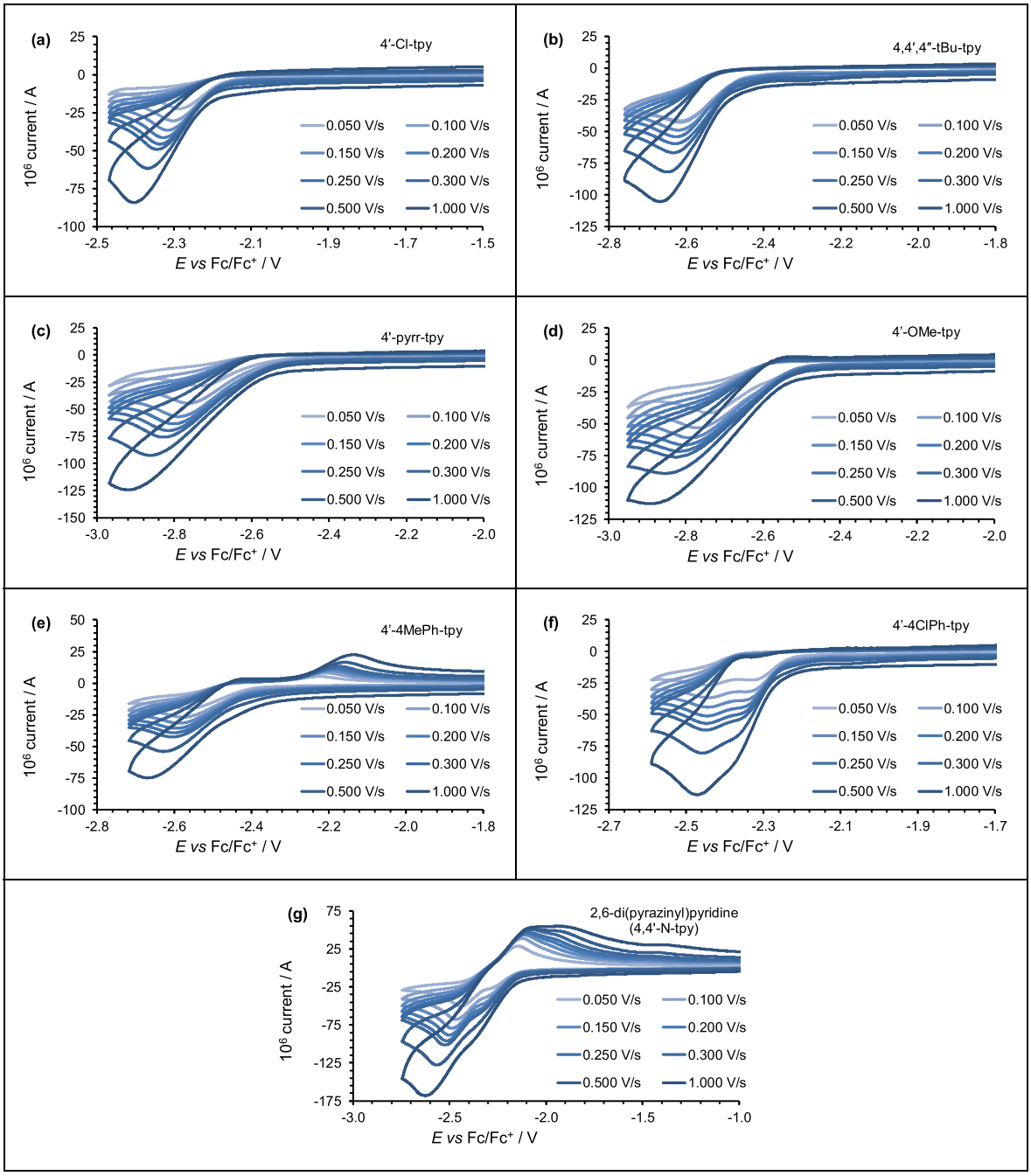

Fig. 4. CVs of a ca 0.002 M DMF solution containing the indicated ligand with 0.1 M TBAHFP as supporting electrolyte, at the indicated scan rates, reported *versus* Fc/Fc^{+}.

constant values with the peak current reduction potential, could be related to the change in geometry that occur during reduction that may occur at different time scales for the different tpy ligands, depending on the type and position of the substituents. Accurate relationships between redox potentials of bis-terpyridine-metal(II) complexes and the combined Hammett constant values were reported, probably since the tpy ligands become flat upon coordination with a metal [17–19,21].

The onset and peak reduction potential of the reduction process of the tpy series, is related to theoretically calculated LUMO energies (E_{LUMO}), electrophilicity index (ω), electrochemical potential (μ) and the calculated reactivity and response indexes "chemical potential governing charge donating process (μ-), chemical potential governing charge accepting process (μ+), electro-donating power (ω-) and electro-accepting power (ω+)" [21] in Fig. 6. The relationships with the onset potential led to higher correlation coefficients (R^2 values) than for the peak reduction potential for the tpy series of this study. This could be related to the difference in broadness of the reduction peak for the different tpy ligands. The results indicate that computed energies and descriptors of the acceptor molecules can be successfully used for the estimation of the expected onset reduction potential of a related tpy ligand.

3.4. Relationships involving reduction potentials of oligo(aza)pyridine ligands

Since the theoretically calculated values correlate well with the experimental reduction potentials for the tpy series, we extended the experimental series to include redox potentials available in literature for

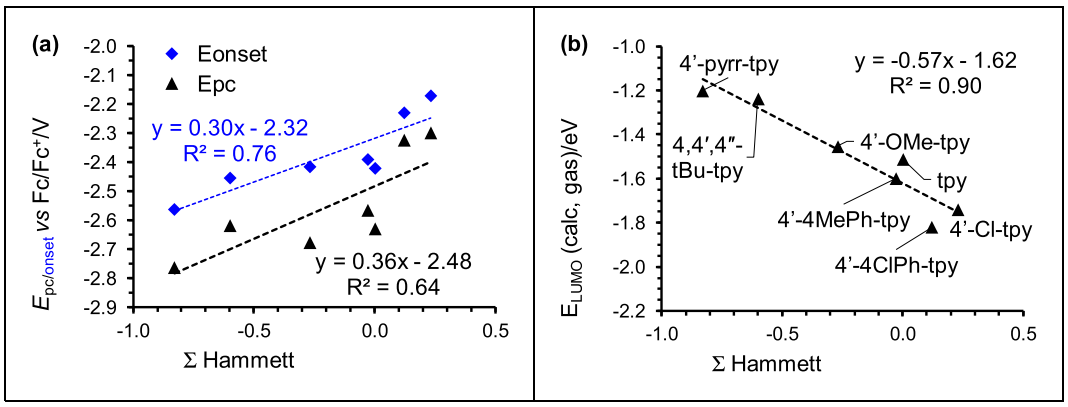

Fig. 5. (a) The relationship between the experimental onset and peak reduction potential (V vs Fc/Fc^{+}) and the sum of the Hammett constants of the substituents on the tpy ligands. (b) The relationship between the energy of the LUMO and the sum of the Hammett constants of the substituents on the tpy ligands. Data in Table 1 and Table 2.

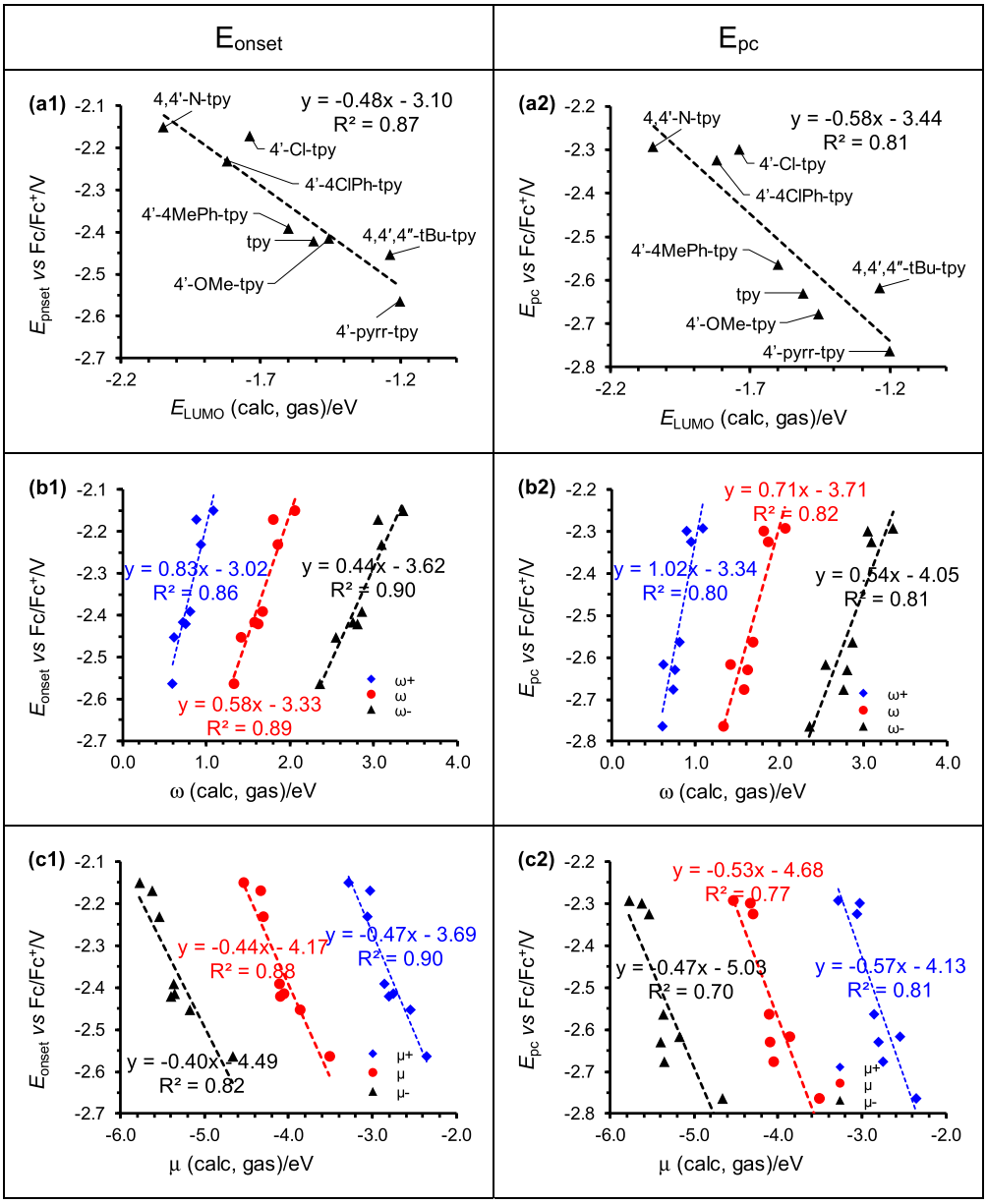

Fig. 6. The relationship between the experimental onset and peak reduction potential (V vs Fc/Fc^{+}) and (a) the energy of the LUMO of the indicated tpy ligands, (b) global electrophilicity index (ω) and (c) chemical potential (μ). Data in Table 2.

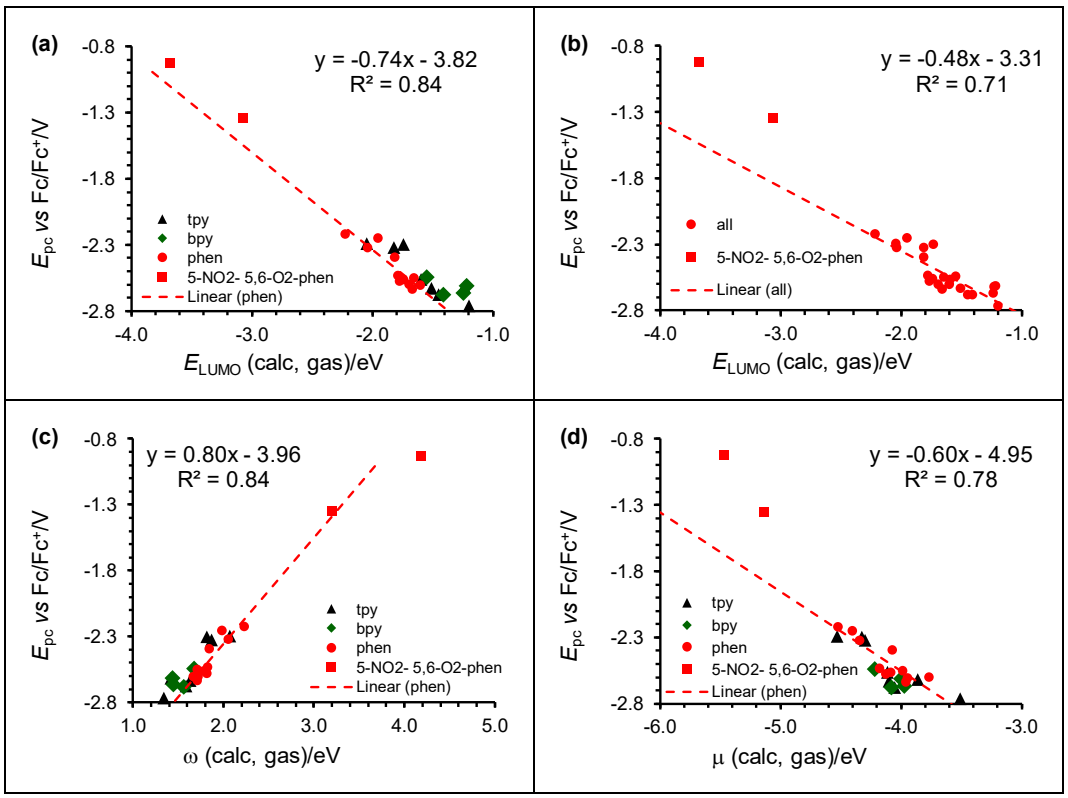

Fig. 7. The relationship between the experimental reduction potential (V vs Fc/Fc^{+}) and the energy of the LUMO of the series of substituted phen, bpy and tpy ligands. (a) Linear line through phen data points, excluding 5-NO2-phen and 5,6-O2-phen. (b) Linear line through phen, tpy and bpy data points, excluding 5-NO2-phen and 5,6-O2-phen. The relationship between the experimental reduction potential (V vs Fc/Fc^{+}) and (c) electrophilicity index (ω) and (d) chemical potential (μ) of the series of substituted phen, bpy and tpy ligands. Data in Table 2.

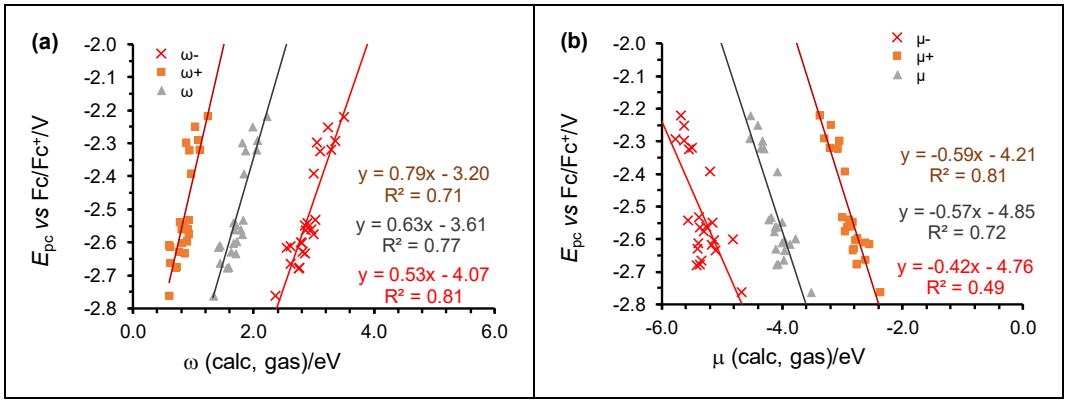

Fig. 8. The relationship between the experimental reduction potential (V vs Fc/Fc^{+}) and the (a) global electrophilicity index (ω) and (b) chemical potential (μ) of the series of substituted phen, bpy and tpy ligands. Data in Table 2.

phen and bpy [11,12], see Fig. 7 for relationships involving LUMO energies and the electrophilicity index and electrochemical potential. The results show that the extended oligo(aza)pyridine series show the same linear trends as the tpy ligands alone. However, the data of bpy, and in some cases also tpy, lies slightly off the linear line if the phen data point are considered alone, see Fig. 7 a, c and d. Data points of 5-NO2-phen and 5,6-O2-phen were excluded from the relationships, since the reduction of these ligand occur on the NO_2 and O [11]. In Fig. 8, the relationships involving the extended poly pyridine series and the different the reactivity and response indexes are shown. The highest correlation coefficients were obtained for the relationships involving the chemical potential governing charge accepting process (μ^{+}) and electro-donating power (ω^{-}). The charge accepting process (μ^{+}) is related to the reduction process and the electro-donating power (ω^{-}) to the nitrogen lone-pair donation of the ligands upon coordination to metals [21].

Depending on the type of ligands considered in the "reduction potentials – LUMO energy (E_{LUMO})" relationships, the correlation coefficient (R^2 value) changes, namely 0.81 (tpy ligands Fig. 6a2), 0.84 (phen ligands Fig. 7 a) and 0.71 (all points Fig. 7 b). Similarly for the "reduction potentials – global electrophilicity index (ω)" relationships, R^2 are 0.82 (tpy ligands Fig. 6b2), 0.84 (phen ligands Fig. 7 c) and 0.77 (all points Fig. 8 a). For the "reduction potentials – chemical potential (μ)" relationships, R^2 are 0.77 (tpy ligands Fig. 6c2), 0.78 (phen ligands Fig. 7 d) and 0.72 (all points Fig. 8 b). All relationships, however, gave $R^2 > 0.77$. The slightly more accurate relationships when only the phen data points are considered, could be related to the fact that no large

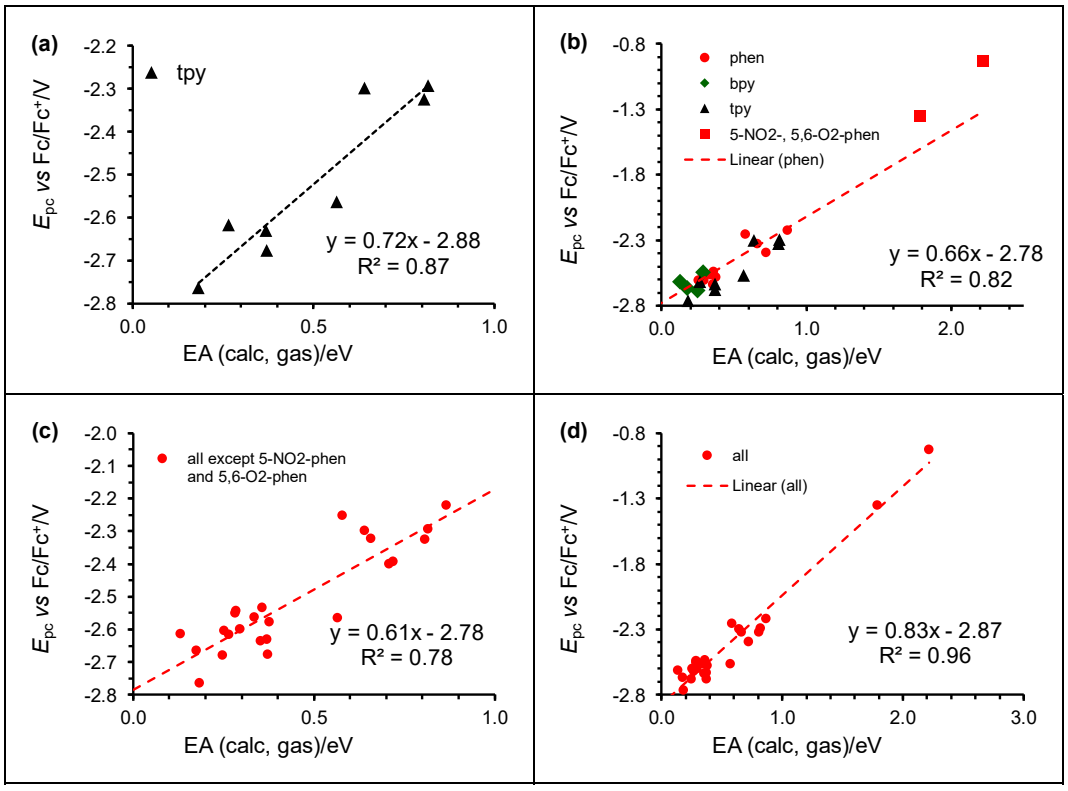

Fig. 9. The relationship between the experimental reduction potential (V vs Fc/Fc^{+}) and the adiabatic electron affinity of (a) the tpy ligands, (b) the phen ligands (c) the series of substituted phen, bpy and tpy ligands excluding NO2-phen and 5,6-O2-phen and (d) the series of substituted phen, bpy and tpy ligands including NO2-phen and 5,6-O2-phen.

geometry change occur for the phen ligands upon reduction; both the neutral and reduced ligands are flat (Fig. 1 d).

The relationships presented in this and the previous section were obtained from data obtained from the optimized neutral ligand only. All the DFT calculated energies and reaction descriptors involved the LUMO energy (energy of the MO where the reduction takes place) and the HOMO energy. The reduction of the substituted tpy, bpy and phen ligands of this study all followed a similar trend when compared to DFT calculated energies and reaction descriptors. Only the data of 5-NO2-phen and 5,6-O2-phen deviated from the trends, since the LUMOs of these ligands are mainly on NO_2 and O [11].

3.5. Theoretical calculated adiabatic electron affinity

Calculated adiabatic electron affinity (EA) values are obtained from the energies from the optimized neutral and reduced ligands. The larger the EA (more positive), the larger the "electron hunger" of the ligand, the easier the reduction process (an electron is taken up easier), thus the more positive is the reduction potential. For the tpy ligands, the peak reduction potential relate to the EA with R^2 value of 0.87, see Fig. 9 (a), slightly higher than the relationship using the data of only the phen ligands ($R^2 = 0.82$), Fig. 9 (b). The similar R^2 value obtained, could be since the energy of the optimized reduced ligand is also used, thus for the tpy ligands, the energy used to change to a more flat geometry upon reduction, is already taken into account. The same relationship, considering the only the phen ligands, or including data of all the ligands (tpy, bpy and phen), give similar linear trends, see Fig. 9 (b) – (d).

3.6. Theoretical calculated reduction potentials

The reduction potential of all the ligands in this study were calculated according to Scheme 3, with the values given on Table 2. To calculate the reduction potential, both the neutral and the reduced ligands were optimized. The relationship between the experimental peak reduction potential (E_{pc}) and the calculated reduction potential ($E_{1/2}$) is given in Fig. 10. In Fig. 10 (a) (E_{pc}) *versus* ($E_{1/2}$) of the phen data points only gives $E_{pc,experimental} = 0.85\ E_{1/2,calculated} - 0.14$ ($R^2 = 0.99$), while in Fig. 10 (b) (E_{pc}) *versus* ($E_{1/2}$) of the all the data points give a very similar relationship, namely $E_{pc,experimental} = 0.85\ E_{1/2,calculated} - 0.13$ ($R^2 = 0.98$). Data for the NO2-phen and 5,6-O2-phen ligands were included here. When excluding the data for NO2-phen and 5,6-O2-phen ligands, Fig. 10 (c), the linear relationship through all data points (except NO2-phen and 5,6-O2-phen) gives $E_{pc,experimental} = 0.91\ E_{1/2,calculated} + 0.04$ ($R^2 = 0.85$) with a slope and intercept nearer to the ideal values of 1 and 0 for a perfect fit. These results show that the reduction potential of oligo(aza)pyridine ligands can be calculated to a high accuracy, with a calculated mean average deviation (MAD) of only 0.066 V (all data points). When only considering the only the ligands of this study, peak reduction potential relate to the calculated reduction potential with a slightly lower value of $R^2 = 0.79$, Fig. 10 (d).

All the relationships between experimental reduction potential and DFT calculated energies E_{LUMO}, ω and μ, were obtained from the DFT energies obtained from the gas phase geometry optimization of the neutral ligand only. To calculate the adiabatic EA, both the neutral and reduced gas phase optimized geometries are needed; thus 2x the computational resources. The "experimental reduction potential – calculated reduction potential" relationships in this section, need ca 3x the computational resources; optimization of the neutral and reduced gas phase geometries, as well as single point solvent calculations are needed.

4. Conclusions

The terpyridine ligands 4′-pyrr-tpy, 4′-OMe-tpy and 4,4″-N-tpy were successfully synthesized and characterized. An irreversible diffusion-controlled reduction process, using cyclic voltammetry, was observed

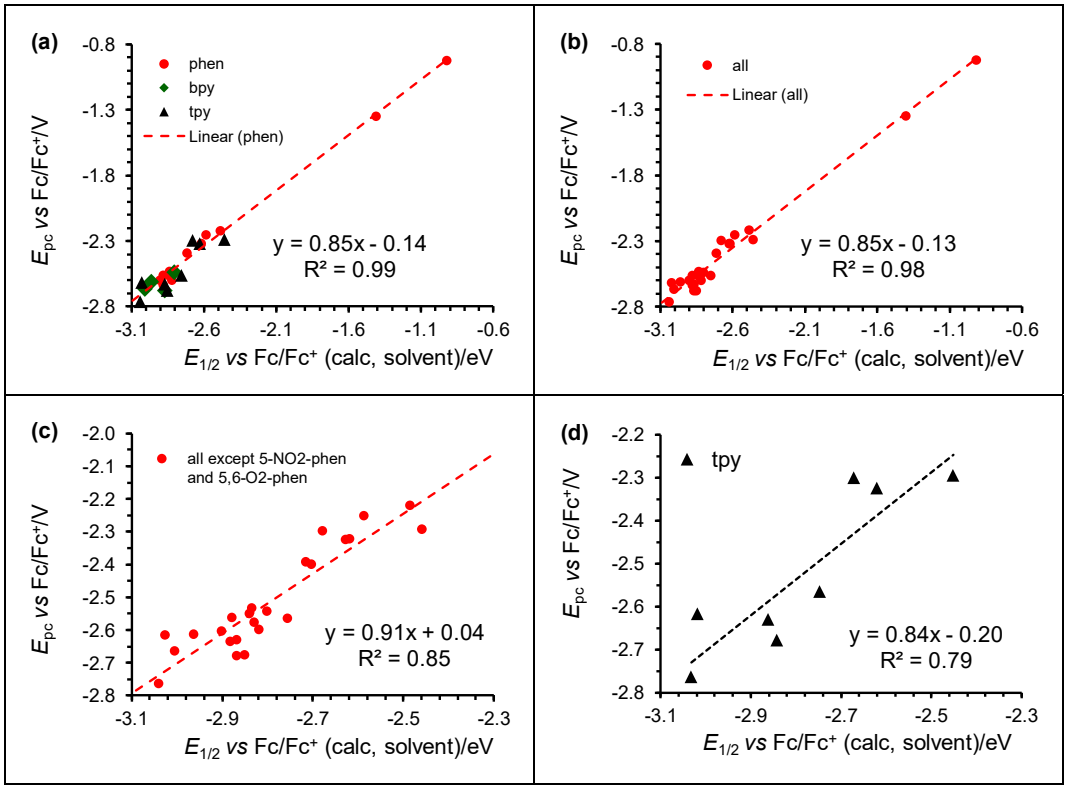

Fig. 10. The relationship between the experimental and calculated reduction potential (V vs Fc/Fc^{+}) of the series of substituted phen, bpy and tpy ligands. (a) Linear relationship through phen data points, y = 0.85x − 0.14 (R^2 = 0.99), (b) Linear relationship through all data points, y = 0.85x − 0.13 (R^2 = 0.98) and (c) Linear relationship through all data points except NO2-phen and 5,6-O2-phen gives y = 0.91x + 0.04 (R^2 = 0.85) with a slope nearer to the ideal value of 1 for a perfect fit. (d) Linear relationship through tpy data points only. Linear relationship through phen data points excluding NO2-phen and 5,6-O2-phen (not shown) gives y = 1.05x + 0.43 (R^2 = 0.95). (d) Linear relationship through tpy data points only gives y = 0.84x − 0.20 (R^2 = 0.79). Data in Table 2.

at a potential below −2.4 V *versus* Fc/Fc^{+}, for a series of 8 differently substituted tpy ligands. The reduction peaks on the CV of tpy ligands are broad with 0.09 – 0.26 V difference between the onset and peak reduction potential. The broadness of the peaks could be related to the change in geometry of the tpy ligand upon reduction; the dihedral between the side pyridines in tpy decreases from 72.5° in the neutral ligand to 25.2° in the reduced tpy. Relationships between the onset reduction potential and DFT calculated energies, gave higher R^2 values than the relationships between peak reduction potential and DFT calculated energies, possibly since the rate of geometry change upon reduction does not influence the onset potential as much as the peak reduction potential. The calculated reduction potential, that takes the energies of both the neutral and the reduced geometry into account, leads to the most accurate "experimental reduction potential – calculated reduction potential" relationship with $R^2 > 0.98$ when all data points are considered.

CRediT authorship contribution statement

Nandisiwe Ghandi Sibongile Mateyise: Data curation, Formal analysis, Writing – review & editing. **Marrigje Marianne Conradie:** Supervision, Resources, Validation, Funding acquisition, Writing – review & editing. **Jeanet Conradie:** Conceptualization, Formal analysis, Supervision, Resources, Validation, Methodology, Funding acquisition, Project administration, Writing – review & editing.

Declaration of Competing Interest

The authors declare that they have no known competing financial interests or personal relationships that could have appeared to influence the work reported in this paper.

Data availability

Data will be made available on request.

Acknowledgements

"This work has received support the South African National Research Foundation (grant numbers 129270 (J.C.), 132504 (J.C.) and 108960 (M.M.C.) and the Central Research Fund of the University of the Free State, Bloemfontein. The High-Performance Computing (HPC) facility of the UFS, the CHPC of South Africa (Grant No. CHEM0947) and the Norwegian Supercomputing Program (Sigma2, Grant No. NN9684K) are acknowledged for computer time."

Ethics Statement

This work does not require any ethical statement.

References

[1] H. Hofmeier, U.S. Schubert, Recent developments in the supramolecular chemistry of terpyridine–metal complexes, Chem. Soc. Rev. 33 (2004) 373–399, https://doi.org/10.1039/B400653B.
[2] C. Wei, Y. He, X. Shi, Z. Song, Terpyridine-metal complexes: Applications in catalysis and supramolecular chemistry, Coord. Chem. Rev. 385 (2019) 1–19, https://doi.org/10.1016/j.ccr.2019.01.005.
[3] J.A. Ramos Sende, C.R. Arana, L. Hernandez, K.T. Potts, M. Keshevarz-K, H. D. Abruna, Electrocatalysis of CO2 reduction in aqueous media at electrodes modified with electropolymerized films of vinylterpyridine complexes of transition metals, Inorg. Chem. 34 (1995) 3339–3348, https://doi.org/10.1021/ic00116a028.
[4] A. Winter, U.S. Schubert, Metal-terpyridine complexes in catalytic application – a spotlight on the last decade, ChemCatChem. 12 (2020) 2890–2941, https://doi.org/10.1002/cctc.201902290.

[5] J.P. Sauvage, J.P. Collin, J.C. Chambron, S. Guillerez, C. Coudret, V. Balzani, F. Barigelletti, L. De Cola, L. Flamigni, Ruthenium(II) and osmium(II) bis (terpyridine) complexes in covalently-linked multicomponent systems: synthesis, electrochemical behavior, absorption spectra, and photochemical and photophysical properties, Chem. Rev. 94 (1994) 993–1019, https://doi.org/10.1021/cr00028a006.

[6] S.G. Shepard, S.M. Fatur, A.K. Rappé, N.H. Damrauer, Highly strained iron(II) polypyridines: exploiting the quintet manifold to extend the lifetime of MLCT excited states, J. Am. Chem. Soc. 138 (2016) 2949–2952, https://doi.org/10.1021/jacs.5b13524.

[7] M.R.S.A. Janjua, Structure-property relationship and systematic study of a series of terpyridine based nonlinear optical compounds: DFT computation of interactive design, J. Clust. Sci. 30 (2019) 45–51, https://doi.org/10.1007/s10876-018-1458-3.

[8] J. Conradie, Polypyridyl copper complexes as dye sensitizer and redox mediator for dye-sensitized solar cells, Electrochem. Commun. 134 (2022), 107182, https://doi.org/10.1016/j.elecom.2021.107182.

[9] N. Armaroli, Photoactive mono- and polynuclear Cu(I)-phenanthrolines. A viable alternative to Ru(II)-polypyridines? Chem. Soc. Rev. 30 (2001) 113–124, https://doi.org/10.1039/b000703j.

[10] M. Grätzel, Conversion of sunlight to electric power by nanocrystalline dye-sensitized solar cells, J. Photochem. Photobiol. A Chem. 164 (2004) 3–14, https://doi.org/10.1016/j.jphotochem.2004.02.023.

[11] H. Ferreira, M.M. Conradie, K.G. von Eschwege, J. Conradie, Electrochemical and DFT study of the reduction of substituted phenanthrolines, Polyhedron. 122 (2017) 147–154, https://doi.org/10.1016/j.poly.2016.11.018.

[12] H. Ferreira, M.M. Conradie, J. Conradie, Electrochemical and electronic properties of a series of substituted polypyridine ligands and their Co(II) complexes, Inorganica Chim. Acta. 486 (2019) 26–35, https://doi.org/10.1016/j.ica.2018.10.020.

[13] G. Ramesh, P. Raghavendra Kumar, M. Pillegowda, G. Periyasamy, P.A. Suchetan, R.J. Butcher, S. Foro, G. Nagaraju, Synthesis, crystal structures, photophysical, electrochemical studies, DFT and TD-DFT calculations and Hirshfeld analysis of new 2,2′:6′,2″-terpyridine ligands with pendant 4′-(trimethoxyphenyl) groups and their homoleptic ruthenium complexes, New J. Chem. 44 (2020) 11471–11489, https://doi.org/10.1039/d0nj00046a.

[14] Q. Zhang, X. Tian, Z. Hu, C. Brommesson, J. Wu, H. Zhou, S. Li, J. Yang, Z. Sun, Y. Tian, K. Uvdal, A series of Zn(II) terpyridine complexes with enhanced two-photon-excited fluorescence for in vitro and in vivo bioimaging, J. Mater. Chem. B 3 (2015) 7213–7221, https://doi.org/10.1039/c5tb01185j.

[15] X. Tian, Q. Zhang, M. Zhang, K. Uvdal, Q. Wang, J. Chen, W. Du, B. Huang, J. Wu, Y. Tian, Probe for simultaneous membrane and nucleus labeling in living cells and in vivo bioimaging using a two-photon absorption water-soluble Zn(ii) terpyridine complex with a reduced π-conjugation system, Chem. Sci. 8 (2016) 142–149, https://doi.org/10.1039/c6sc02342h.

[16] M.R.S.A. Janjua, W. Guan, L. Yan, Z.M. Su, M. Ali, I.H. Bukhari, Prediction of robustly large molecular second-order nonlinear optical properties of terpyridine-substituted hexamolybdates: Structural modelling towards a rational entry to NLO materials, J. Mol. Graph. Model. 28 (2010) 735–745, https://doi.org/10.1016/j.jmgm.2010.01.011.

[17] J. Chambers, B. Eaves, D. Parker, R. Claxton, P.S. Ray, S.J. Slattery, Inductive influence of 4′-terpyridyl substituents on redox and spin state properties of iron(II) and cobalt(II) bis-terpyridyl complexes, Inorganica Chim. Acta 359 (2006) 2400–2406, https://doi.org/10.1016/j.ica.2005.12.065.

[18] J.C. Dickenson, M.E. Haley, J.T. Hyde, Z.M. Reid, T.J. Tarring, D.A. Iovan, D. P. Harrison, Fine-tuning metal and ligand-centered redox potentials of homoleptic bis-terpyridine complexes with 4′-aryl substituents, Inorg. Chem. 60 (2021) 9956–9969, https://doi.org/10.1021/acs.inorgchem.1c01233.

[19] M. Sjödin, J. Gätjens, L.C. Tabares, P. Thuéry, V.L. Pecoraro, S. Un, Tuning the redox properties of manganese(II) and its implications to the electrochemistry of manganese and iron superoxide dismutases, Inorg. Chem. 47 (2008) 2897–2908, https://doi.org/10.1021/ic702428s.

[20] L.J. Kershaw Cook, F. Tuna, M.A. Halcrow, Iron(ii) and cobalt(ii) complexes of tris-azinyl analogues of 2,2′:6′,2″-terpyridine, Dalt. Trans. 42 (2013) 2254–2265, https://doi.org/10.1039/c2dt31736b.

[21] V. Ramírez-Delgado, M. Cruz-Ramirez, L. Felipe Hernández-Ayala, Y. Reyes-Vidal, R. Patakfalvi, J. Carlos García-Ramos, F.J. Tenorio, L. Ruiz-Azuara, L. Ortiz-Frade, The role of the π acceptor character of polypyridine ligands on the electrochemical response of Co(II) complexes and its effect on the homogenous electron transfer rate constant with the enzyme glucose oxidase, J. Mex. Chem. Soc. 59 (2015) 282–293. http://www.redalyc.org/articulo.oa?id=47545630006.

[22] L.A. Ortiz-Frade, L. Ruiz-Ramírez, I. González, A. Marín-Becerra, M. Alcarazo, J. G. Alvarado-Rodriguez, R. Moreno-Esparza, Synthesis and spectroelectrochemical studies of mixed heteroleptic chelate complexes of ruthenium(II) with 1,8-Bis(2-pyridyl)-3,6-dithiaoctane (pdto) and substituted 1,10-phenanthrolines, Inorg. Chem. 42 (2003) 1825–1834, https://doi.org/10.1021/ic025849q.

[23] H. Ferreira, K.G. von Eschwege, J. Conradie, Electronic properties of Fe charge transfer complexes – a combined experimental and theoretical approach, Electrochim. Acta. 216 (2016) 339–346, https://doi.org/10.1016/j.electacta.2016.09.034.

[24] K.G. von Eschwege, J. Conradie, Iron phenanthrolines: a density functional theory study, Inorganica Chim. Acta 471 (2018) 391–396, https://doi.org/10.1016/j.ica.2017.11.047.

[25] D. van der Westhuizen, K.G. von Eschwege, J. Conradie, Electrochemistry and spectroscopy of substituted [Ru(phen)3]2+ and [Ru(bpy)3]2+ complexes, Electrochim. Acta. 320 (2019), https://doi.org/10.1016/j.electacta.2019.07.051.

[26] D. Westhuizen, J. Conradie, K.G. Eschwege, Electrochemistry of Os bipyridyl and phenanthroline complexes, comparison with Ru and Fe, Electroanalysis. 32 (2020) 2838–2851, https://doi.org/10.1002/elan.202060300.

[27] Z. Mtshali, K.G. von Eschwege, J. Conradie, Electrochemical study of the Mn(II/III) oxidation of tris(polypyridine)manganese(II) complexes, Electrochim. Acta. (2021), 138965, https://doi.org/10.1016/j.electacta.2021.138965.

[28] H. Ferreira, M.M. Conradie, J. Conradie, Electrochemical properties of a series of Co(II) complexes, containing substituted phenanthrolines, Electrochim. Acta. 292 (2018) 489–501, https://doi.org/10.1016/j.electacta.2018.09.151.

[29] J. Conradie, DFT Study of bis(1,10-phenanthroline)copper complexes: molecular and electronic structure, redox and spectroscopic properties and application to Solar Cells, Electrochim. Acta. (2022), 140276, https://doi.org/10.1016/j.electacta.2022.140276.

[30] G. Sanna, M.I. Pilo, M.A. Zoroddu, R. Seeber, S. Mosca, Electrochemical and spectroelectrochemical study of copper complexes with 1,10-phenanthrolines, Inorganica Chim. Acta. 208 (1993) 153–158, https://doi.org/10.1016/S0020-1693(00)85115-4.

[31] E. Chiyindiko, E.H.G. Langner, J. Conradie, Electrochemical behaviour of copper (II) complexes containing 2-hydroxyphenones, Electrochim. Acta. 424 (2022), 140629, https://doi.org/10.1016/j.electacta.2022.140629.

[32] G. Gritzner, J. Kuta, Recommendations on reporting electrode potentials in nonaqueous solvents (Recommendations 1983), Pure Appl. Chem. 56 (1984) (1983) 461–466, https://doi.org/10.1351/pac198456040461.

[33] M.J. Frisch, G.W. Trucks, H.B. Schlegel, G.E. Scuseria, M.A. Robb, J.R. Cheeseman, G. Scalmani, V. Barone, G.A. Petersson, H. Nakatsuji, X. Li, M. Caricato, A. V. Marenich, J. Bloino, B.G. Janesko, R. Gomperts, B. Mennucci, H.P. Hratchian, J. V. Ortiz, A.F. Izmaylov, J.L. Sonnenberg, D. Williams-Young, F. Ding, F. Lipparini, F. Egidi, J. Goings, B. Peng, A. Petrone, T. Henderson, D. Ranasinghe, V.G. Zakrzewski, J. Gao, N. Rega, G. Zheng, W. Liang, M. Hada, M. Ehara, K. Toyota, R. Fukuda, J. Hasegawa, M. Ishida, T. Nakajima, Y. Honda, O. Kitao, H. Nakai, T. Vreven, K. Throssell, J. Montgomery, J. A., J.E. Peralta, F. Ogliaro, M.J. Bearpark, J.J. Heyd, E.N. Brothers, K.N. Kudin, V.N. Staroverov, T.A. Keith, R. Kobayashi, J. Normand, K. Raghavachari, A.P. Rendell, J.C. Burant, S.S. Iyengar, J. Tomasi, M. Cossi, J.M. Millam, M. Klene, C. Adamo, R. Cammi, J.W. Ochterski, R.L. Martin, K. Morokuma, O. Farkas, J.B. Foresman, D.J. Fox, Gaussian 16, Revision B.01, (2016).

[34] A.D. Becke, Density-functional exchange-energy approximation with correct asymptotic behavior, Phys. Rev. A 38 (1988) 3098–3100, https://doi.org/10.1103/PhysRevA.38.3098.

[35] C. Lee, W. Yang, R.G. Parr, Development of the Colle-Salvetti correlation-energy formula into a functional of the electron density, Phys. Rev. B 37 (1988) 785–789, https://doi.org/10.1103/PhysRevB.37.785.

[36] Chemcraft - graphical software for visualization of quantum chemistry computations., (n.d.). http://www.chemcraftprog.com/.

[37] T. Koopmans, Über die Zuordnung von Wellenfunktionen und Eigenwerten zu den Einzelnen Elektronen Eines Atoms, Physica. 1 (1934) 104–113, https://doi.org/10.1016/S0031-8914(34)90011-2.

[38] J. Conradie, A Frontier orbital energy approach to redox potentials, J. Phys. Conf. Ser. 633 (2015), 012045, https://doi.org/10.1088/1742-6596/633/1/012045.

[39] R.S. Mulliken, A new electroaffinity scale; Together with data on valence states and on valence ionization potentials and electron affinities, J. Chem. Phys. 2 (1934) 782–793, https://doi.org/10.1063/1.1749394.

[40] M.V. Putz, N. Russo, E. Sicilia, About the Mulliken electronegativity in DFT, Theor. Chem. Acc. 114 (2005) 38–45, https://doi.org/10.1007/s00214-005-0641-4.

[41] F. De Proft, W. Langenaeker, P. Geerlings, Ab initio determination of substituent constants in a density functional theory formalism: calculation of intrinsic group electronegativity, hardness, and softness, J. Phys. Chem. 97 (1993) 1826–1831, https://doi.org/10.1021/j100111a018.

[42] R.G. Parr, L.V. Szentpály, S. Liu, Electrophilicity index, J. Am. Chem. Soc. 121 (1999) 1922–1924, https://doi.org/10.1021/ja983494x.

[43] J.L. Gázquez, A. Cedillo, A. Vela, Electrodonating and electroaccepting powers, J. Phys. Chem. A. 111 (2007) 1966–1970, https://doi.org/10.1021/jp065459f.

[44] J.L. Gázquez, Perspectives on the density functional theory of chemical reactivity, J. Mex. Chem. Soc. 52 (2008) 3–10. http://www.scielo.org.mx/scielo.php?script=sci_arttext&pid=S1870-249X2008000100002.

[45] J. Conradie, Redox chemistry of bis(terpyridine)manganese(II) complexes – a molecular view, J. Electroanal. Chem. 913 (2022), 116272, https://doi.org/10.1016/j.jelechem.2022.116272.

[46] J. Conradie, Redox chemistry of tris(β-diketonate)cobalt(III) complexes: a molecular view, J. Electrochem. Soc. 169 (4) (2022) 046522.

[47] A.V. Marenich, J. Ho, M.L. Coote, C.J. Cramer, D.G. Truhlar, Computational electrochemistry : prediction of liquid-phase reduction potentials †, Phys. Chem. Chem. Phys. 16 (2014) 15068–15106, https://doi.org/10.1039/c4cp01572j.

[48] M. Namazian, C.Y. Lin, M.L. Coote, Benchmark calculations of absolute reduction potential of ferricinium/ferrocene couple in nonaqueous solutions, J. Chem. Theory Comput. 6 (2010) 2721–2725, https://doi.org/10.1021/ct1003252.

[49] A.V. Marenich, C.J. Cramer, D.G. Truhlar, Universal solvation model based on solute electron density and on a continuum model of the solvent defined by the bulk dielectric constant and atomic surface tensions, J. Phys. Chem. B. 113 (2009) 6378–6396, https://doi.org/10.1021/jp810292n.

[50] R.E. Skyner, J.L. McDonagh, C.R. Groom, T. van Mourik, J.B.O. Mitchell, A review of methods for the calculation of solution free energies and the modelling of systems in solution, Phys. Chem. Chem. Phys. 17 (9) (2015) 6174–6191.

[51] J. Ferrando-Soria, O. Fabelo, M. Castellano, J. Cano, S. Fordham, H.C. Zhou, Multielectron oxidation in a ferromagnetically coupled dinickel(II) triple mesocate, Chem. Commun. 51 (2015) 13381–13384, https://doi.org/10.1039/c5cc03544a.
[52] N. Elgrishi, K.J. Rountree, B.D. McCarthy, E.S. Rountree, T.T. Eisenhart, J. L. Dempsey, A practical beginner's guide to cyclic voltammetry, J. Chem. Educ. 95 (2018) 197–206, https://doi.org/10.1021/acs.jchemed.7b00361.
[53] C. Hansch, A. Leo, R.W. Taft, A survey of Hammett substituent constants and resonance and field parameters, Chem. Rev. 91 (1991) 165–195, https://doi.org/10.1021/cr00002a004.